PROCEEDINGS OF SPIE

SPIEDigitalLibrary.org/conference-proceedings-of-spie

The high-contrast performance of an optical vortex coronagraph

Palacios, David, Swartzlander, G.

David M. Palacios, G. A. Swartzlander Jr., "The high-contrast performance of an optical vortex coronagraph," Proc. SPIE 6288, Current Developments in Lens Design and Optical Engineering VII, 62880B (31 August 2006); doi: 10.1117/12.682088

SPIE.

Event: SPIE Optics + Photonics, 2006, San Diego, California, United States

Downloaded From: https://www.spiedigitallibrary.org/conference-proceedings-of-spie on 02 Mar 2022 Terms of Use: https://www.spiedigitallibrary.org/terms-of-use

The High Contrast Performance of an Optical Vortex Coronagraph

David M. Palacios[1] and G.A. Swartzlander Jr.[2]

[1]*Jet Propulsion Laboratory*

California Institute of Technology

4800 Oak Grove Dr., Pasadena, CA 91109

David.M.Palacios@jpl.nasa.gov

[2]*The School of Optical Sciences*

The University of Arizona

1630 E. University Blvd., Tucson, AZ 85721

grovers@u.arizona.edu

ABSTRACT

The goal of the Terrestrial Planet Finder Mission is to detect and characterize Earth-like planets. Detection of these faint objects, which appear very close to their parent stars, requires a coronagraph capable of achieving better than 10^{-10} starlight suppression within a few Airy rings of the stellar image. The coronagraph is also required to maintain this high stellar extinction over a 100nm spectral bandwidth. To ease requirements on the telescope, a high planet light throughput and low sensitivity to wave front aberrations are also desirable features. An optical vortex coronagraph is a promising candidate architecture, which makes use of a spiral phase plate placed in an intermediate image plane to null out the stellar signal. This architecture has the advantage of high stellar extinction, high planet light throughput, and low sensitivity to wave front aberrations. Here we report the high contrast performance of an optical vortex coronagraph limited by the manufacturability of the spiral phase plate.

Keywords: coronagraphs; terrestrial planets; optical vortices;

1. INTRODUCTION

The Terrestrial Planet Finder Coronagraph (TPF-C) is a proposed space telescope designed to detect and characterize a terrestrial planet in visible light (500-800nm). Presently, TPF-C is designed[1] to provide at least 10^{-10} starlight

Current Developments in Lens Design and Optical Engineering VII, edited by Pantazis Z. Mouroulis, Warren J. Smith, R. Barry Johnson, Proc. of SPIE Vol. 6288, 62880B, (2006) · 0277-786X/06/$15 · doi: 10.1117/12.682088

Downloaded From: https://www.spiedigitallibrary.org/conference-proceedings-of-spie on 02 Mar 2022
Terms of Use: https://www.spiedigitallibrary.org/terms-of-use

suppression with a stability of 2.5×10^{-11} at an inner working angle of $4\lambda/D$ where D is the longest dimension of the primary mirror* and λ_0=550nm is the telescopes optimal operating wavelength.

In order to meet these tight requirements several coronagraph designs have been studied[2-5]. Trauger[6] et al. have demonstrated high contrast ($\sim 10^{-9}$) monochromatic light suppression of an on-axis source by using a band-limited mask in conjunction with a wave-front control system on the High Contrast Imaging Test Bed (HCIT) at JPL. However, the most successful band-limited mask used on HCIT (a linear sinc^2 mask) was designed for an operating wavelength, λ_0=800nm. Broadband operation between 500-800nm has not yet been demonstrated.

The HCIT linear sinc^2 mask belongs to a family of occulting masks known as 4^{th} order masks. Named thusly because the intensity of the residual light, post coronagraph, exhibits a 4^{th} order dependence to a tip/tilt aberration in the entrance pupil. Kucher[7] et al devised a way to create a mask with an 8^{th} order sensitivity to tip/tilt by combining two properly weighted and arranged linear sinc^2 functions. However, this comes at the price of reduced planet light throughput in comparison to the starlight throughput. The high contrast performance of these masks is currently under investigation on HCIT at JPL.

An Optical Vortex Coronagraph (OVC) is a new type of high contrast imaging technique under investigation for TPF-C. In an OVC the amplitude mask typically found in a Lyot Coronagraph is replaced with a spiral etched phase plate known as an optical vortex mask (OVM). In an ideal OVC the light from a star is canceled over the entire pupil increasing the planet light throughput and decreasing the inner working angle of the telescope[8]. In addition, an OVC is less sensitive to low-order wave front aberrations of the entrance pupil than the previously investigated 8^{th} order band-limited masks[9]. Recently, Lee et al.[10] experimentally demonstrated the low-contrast application of an OVC with a high level of on-axis source attenuation over the entire pupil. Swartzlander[11] also designed an achromatic OVM for low-contrast applications. Using a similar technique it may be possible to produce an achromatic OVM suitable for high contrast applications.

This paper addresses the high contrast performance of an OVC limited by the manufacturability of the OVM. The ideal OVC previously examined[8-11] contained a smoothly varying OVM. However, the spiral phase shape of a real OVM will be pixilated by the lithography technique used to etch it. In this paper, we will present simulations of an OVC containing an OVM etched with a 0.2 micron pixel size, which is within the limits of present lithography techniques.[12-14]

* The primary mirror is designed to have an elliptical shape with the major axis equal to 8m and the minor axis equal to 3.5m.

Downloaded From: https://www.spiedigitallibrary.org/conference-proceedings-of-spie on 02 Mar 2022
Terms of Use: https://www.spiedigitallibrary.org/terms-of-use

We will present the predicted high contrast performance of an OVC as well as the optimized power throughput of a planet separated by its host star by an angle of 2λ/D and 4λ/D.

2. WHAT IS AN OPTICAL VORTEX?

Vortices are a fascinating phenomenon of waves in nature and are known to occur in many physical systems[15-17]. In optical systems, vortices may be characterized as dark cores of destructive interference that occur at phase singularities in beams of spatially coherent light. This dark core may be used to attenuate an on-axis source so nearby objects may be detected[18]. An optical vortex embedded in the center of a scalar, monochromatic beam of light propagating in the z direction may be described by an electric field written in cylindrical coordinates (ρ, ϕ, z)[17]:

$$E(\rho,\ \phi,\ z,\ t) = A(\rho,\ z)\exp(im\phi)\exp(i\omega t - ikz) \tag{1}$$

where A(ρ, z) is a circularly symmetric amplitude function, m is a signed integer known as the topological charge of the vortex, and k=2π/λ is the wave number of a monochromatic field of wavelength λ. The field described by Eq. (1), is said to possess vorticity because at any fixed instant of time, helical surfaces of constant phase given by mϕ–kz=const are produced for integer values of m. Along the axis of this helix (ρ=0) the amplitude vanishes owing to destructive interference in the vicinity of the vortex core i.e., A(0, z)=0. The topological charge of the vortex is given by[17]:

$$m = (1/2\pi)\oint \nabla\phi\, ds \tag{2}$$

where ∇ϕ is the phase gradient and ds is a line enclosing the helix axis of the vortex. Optical vortices may be created by a variety of different methods[17]. The technique most germane to coronagraphy is the use of an OVM a type of diffractive optical element, which we will describe in the next section.

3. AN OPTICAL VORTEX MASK

A monochromatic, planar (m=0) beam of amplitude E_0 may be converted into a vortex beam by transmitting the light through a transparent diffractive phase mask having a thickness that varies azimuthally. The change in thickness of an OVM is given by[19],

$$dz = m\lambda_0 d\phi / 2\pi(n_s - n_0) \tag{3}$$

Downloaded From: https://www.spiedigitallibrary.org/conference-proceedings-of-spie on 02 Mar 2022
Terms of Use: https://www.spiedigitallibrary.org/terms-of-use

where $d\phi$ is an azimuthal rotation about the center of the OVM (in units of radians), λ_0 is the wavelength for which the mask is intended, n_s is the refractive index of the substrate, and n_0 is the index of refraction of the surrounding medium. A three dimensional plot of an OVM may be seen in Fig. 1.

Light passing through an OVM gains an azimuthally varying phase as stated above, but in order for the transmitted field to be physical[17], the amplitude must be zero along the axis of the helical phase front. This central dark spot is known as the optical vortex core. Like the eye of a hurricane, the vortex core created by an OVM has a physical extent, which may be derived using a simple ray model as illustrated in Fig. 2. A ray is perpendicularly incident on the flat backside of the OVM a distance ρ from the center of the mask and at an angle $d\phi$ from the edge of the deepest etch. The ray passes through the OVM glass substrate of refractive index n_s and refracts at the spiral shaped output side of the OVM into the surrounding medium of refractive index n_0. Using geometry it is possible to show that the angle of incidence (γ_ϕ) between the ray and the spiral surface is given by,

$$\gamma_\phi = \tan^{-1}\left[dz/\rho d\phi\right] \tag{4}$$

Substituting Eq. (3) into Eq(4) yields:

$$\gamma_\phi = \tan^{-1}\left[m\lambda_0/2\pi\rho\left(n_s - n_0\right)\right] \tag{5}$$

By examining Eq. (5) we can deduce that the closer the ray is to the center of the mask ($\rho \to 0$) the larger the value of γ_ϕ. The ray will totally internally reflect (TIR) when $\gamma_\phi = \gamma_{TIR} = \sin^{-1}[n_0/n_s]$.[20] It is possible to derive the vortex core size, ρ_c, for an optical vortex created by an OVM by solving for ρ in Eq (5) and setting $\gamma_\phi = \gamma_{TIR}$:

$$\rho_c = m\lambda_0/2\pi\left(n_s - n_0\right)\tan\left[\gamma_{TIR}\right] \tag{6}$$

All rays incident on the mask within ρ_c totally internally reflect and the transmitted amplitude is zero.

However, this does not completely represent the amplitude transmission of an OVM. When an electromagnetic field is incident on an interface between two dielectric mediums the amplitudes of the reflected and transmitted portions of the field will vary with the angle of incidence and the polarization state of the impinging light[20]. Referring to the geometry depicted in Fig. 2, if the electric field is perpendicular to the plane of incidence (defined by the incident ray and the spiral surface) it is radially polarized (E_ρ) and if the electric field is parallel to the plane of incidence it is azimuthally polarized (E_ϕ). The relative amplitude of the transmitted radially polarized light for $\rho > \rho_c$ is given by:

$$\frac{E_\rho}{E_0} = 1 - \frac{n_s\cos\left(\gamma_\phi\right) - \frac{\mu_s}{\mu_0}\sqrt{n_0^{\,2} - n_s^{\,2}\sin^2\left(\gamma_\phi\right)}}{n_s\cos\left(\gamma_\phi\right) + \frac{\mu_s}{\mu_0}\sqrt{n_0^{\,2} - n_s^{\,2}\sin^2\left(\gamma_\phi\right)}} \tag{7}$$

Downloaded From: https://www.spiedigitallibrary.org/conference-proceedings-of-spie on 02 Mar 2022
Terms of Use: https://www.spiedigitallibrary.org/terms-of-use

where μ_0 is the magnetic permeability of free space and μ_s is the magnetic permeability of the OVM substrate material. The relative amplitude of the transmitted azimuthally polarized light for $\rho > \rho_c$ is given by:

$$\frac{E_\phi}{E_0} = 1 - \frac{\frac{\mu_s}{\mu_0} n_0^{\,2} \cos(\gamma_\phi) - n_s \sqrt{n_0^{\,2} - n_s^{\,2} \sin^2(\gamma_\phi)}}{\frac{\mu_s}{\mu_0} n_0^{\,2} \cos(\gamma_\phi) + n_s \sqrt{n_0^{\,2} - n_s^{\,2} \sin^2(\gamma_\phi)}} \tag{8}$$

Radial line plots of the amplitude transmission of OVMs of topological charge, m=2,4, and 6 are compared in Fig. 3. Although the line plots of the radial and azimuthal polarizations seen in Fig. 3 look very similar they are slightly different. When linearly polarized light is considered, this leads to a small asymmetry in the vortex core shape. For linear polarized light, the vortex core will be slightly elongated along the axis perpendicular to the polarization state. This will have a small effect on the performance of the coronagraph that should be noted, although it will be a much smaller effect than the discretization of the OVM.

Previous work on an OVC assumed an ideal OVM with a smooth varying spiral. However, a real OVM will possess a descretized spiral because the etching techniques used to carve the spiral have a minimum etch able feature size. The OVM is a mode converter, and converts the planer non-vortex mode of the telescope into a desired vortex mode of topological charge, m. When the OVM is not manufactured to the desired ideal smooth spiral, the mode conversion will not be complete and other modes of topological charge, $m' \neq m$, will also be created. This includes a non-vortex mode (m=0), which will cause stellar light leakage in the OVC. Using present ion-beam lithography techniques it is possible to etch an m=6 OVM for a wavelength of λ_0=600nm, with a minimum etchable feature size of approximately 50nm.* Due to simulation array size constraints (4096 x 4096 arrays) the numerical simulations presented in Section 5 contain an OVM with a mask feature size of 0.2 microns.

4. CORONAGRAPH ARCHITECTURE

A simple unfolded architecture of an OVC is depicted in Fig. 4. Light from a distant star is imaged by a telescope represented by L_1. An OVM of topological charge m is placed near the focus of L_1 and a collimator represented by L_2

* Using advanced techniques currently under investigation at JPL it is possible to smooth features without the use of smaller etchable feature sizes[12-14].

Downloaded From: https://www.spiedigitallibrary.org/conference-proceedings-of-spie on 02 Mar 2022
Terms of Use: https://www.spiedigitallibrary.org/terms-of-use

re-images the entrance pupil of the telescope system after the starlight is transmitted through the OVM. A circular Lyot stop is placed at the re-imaged pupil blocking unwanted starlight at the edge of the pupil. The remaining light is then re-imaged by L_3 with the on-axis starlight greatly attenuated compared to the off-axis light from a planet.

In this paper, I will assume circular instead of elliptical symmetry since the present TPF-C telescope design contains beam-circularizing optics to increase the efficacy of the wave-front control system. Therefore, ignoring polarization effects, the optimal Lyot stop is a circular aperture.

5. NUMERICAL SIMULATIONS

The high contrast performance of an OVC was simulated with an ideal imaging system possessing the following parameters:

- All simulations were performed on a 4096x4096 grid array.
- The OVM was designed to produce either an m=2,4, or 6 charged vortex at λ_0= 600nm.
- D=100 pixels.
- The focal plane profile of lens L_1 in Fig. 4 was assumed to be an ideal Airy disk before application of the OVM.
- The first zero of the Airy disk mentioned above, had a radius of 51 pixels.
- The L_1 imaging system had an f# = 27, which matches the design of HCIT at JPL.
- The amplitude transmission function of the OVM was an incoherent superposition of Eq. (7) and Eq, (8) assuming E_0=1.
- μ_s=μ_0=1.
- n_s=1.5 and n_0=1.
- The OVM was discretized with a mask feature size of 0.2 microns.
- Contrast as defined by Green[21] et al. was used as a metric of system performance.

Simulated OVC Lyot plane images for an on-axis star are shown in Fig. 5. One remarkable feature of an ideal OVC is its ability to null over the entire pupil when m is an even integer[8, 22]. The discretization of the OVM causes leakage of stellar light reducing this effect. However, even with the discretized OVM the power inside the pupil was

Downloaded From: https://www.spiedigitallibrary.org/conference-proceedings-of-spie on 02 Mar 2022
Terms of Use: https://www.spiedigitallibrary.org/terms-of-use

reduced by several orders of magnitude and we were able to verify the Lyot plane intensity profile predicted by Foo et al.[8] (for the m=2 case) and by Mawet et al.[22].

TPF-C is presently designed to have an inner working angle of 4λ/D. This requires the use of an 8m diameter primary mirror, which is costly and difficult to manufacture. If TPF-C could have an inner working angle of 2λ/D, a 4m diameter primary mirror could be used, which would greatly reduce the cost and difficulty in manufacturing the mirror. Since an OVC is able to null such a large area of the pupil we optimized the performance of the OVC to obtain a contrast below 10^{-10} at 2λ/D. When the OVC contains a discretized OVM the Lyot stop size must be reduced to optimize the system for high contrast performance. The average contrast between 2-3λ/D vs. the Lyot stop diameter is plotted in Fig. 6(a) for m=2,4, and 6 OVCs. Using these results, we may conclude that a contrast below 10^{-10} at 2λ/D may be obtained by an m=4 OVC and an m=6 OVC by reducing the Lyot diameter to 0.8D. To compare these results to other coronagraph architectures, the average contrast between 4-5λ/D vs. the Lyot stop diameter is plotted in Fig. 6(b). The results show a similar trend although better starlight suppression is obtained in general and now the m=2 OVC performs better than the required 10^{-10} contrast required for terrestrial planet detection.

Another important quantity to consider is the amount of planet light that is transmitted through the system to the final image plane. A coronagraph may obtain high levels of contrast between a star and a planet but still fail to detect a planet because so few planet photons make it through the system. Besides this minimum detectable signal limitation, it is always desirable to increase the signal from the planet because this will decrease the image integration time. This increases the scientific gain that may be achieved within the mission's lifetime. Planet light throughput may be defined as the amount of planet light power transmitted through the Lyot stop. It's reduced primarily from the Lyot stop but may also be reduced by the on-axis vortex core as well. In addition, the planet light throughput will decrease for OVCs that employ higher m value OVMs, because the size of the vortex core increases with topological charge (see Fig. 3). The planet light throughput vs. Lyot stop size for m=0,2,4, and 6 OVCs are plotted in Fig. 7 for (a) a planet/star separation of 2λ/D and (b) a planet/star separation of 4λ/D. The m=0 plot in Fig. 7 is the no OVM case and represents the maximum power the Lyot stop alone will allow through the system. These results verify our expectation that the planet light throughput decreases as the value of m increases. The plots also show that the Lyot stop throughput itself is the dominant degrader of planet light throughput for smaller Lyot stop sizes. For an m=4 OVC with D_L=0.8D, a planet

Downloaded From: https://www.spiedigitallibrary.org/conference-proceedings-of-spie on 02 Mar 2022
Terms of Use: https://www.spiedigitallibrary.org/terms-of-use

separated from its host star by $2\lambda/D$ had a throughput of $0.53P_T$, where P_T is the total planet light power. A planet separated from its host star by $4\lambda/D$ had a throughput of $0.62P_T$.

6. CONCLUSIONS

An OVC employing an OVM etched by today's ion-beam technology is able to achieve the 10 order of magnitude starlight suppression required of TPF-C. Our simulations verify the Lyot plane behavior of an OVC predicted by Foo et al.[8] and Mawet et al.[22]. An m=4 OVC with D_L=0.8D, reached the required 10^{-10} starlight suppression and obtained a planet light thoughput of $0.53P_T$ for a planet separated from its host star by $2\lambda/D$.

An OVC may hold several key advantages for TPF-C. These advantages include high planet light throughput, manufacturability, lower aberration sensitivity[9], and possible broadband operation[11]. Vortex masks with topological charge ranging from m=1-3 have been manufactured[13,14]. Using present ion-beam lithography techniques, it may be possible to construct an m=6 vortex mask designed for an optical wavelength of λ_0=600nm.

ACKNOWLEDGMENTS

I would like to thank S. Shaklan and D. Wilson for their suggestions and comments. This work was carried out at the Jet Propulsion Laboratory, California Institute of Technology, under contract with the National Aeronautics and Space Administration.

REFERENCES

[1] Ford, V.G., et al. Proc. SPIE **5487**, 1274 (2004).

[2] Kasdin, N.J., Vanderbei, R.J. Spergel, D.N., and Littman, M.G., ApJ **582**, 1147 (2004).

[3] Guyon, O., A&A **404**, 379 (2003).

[4] Rouan, D., Bocceletti, A. Riaud, P., and Baudrand, J. Proc. SPIE **4860**, 192 (2003).

[5] Kuchner, M.J., and Traub, W.A., ApJ, **570**, 900 (2002).

[6] Trauger, J.T. et al., Proc. SPIE **5487**, 1330 (2004).

[7] Kuchner, M.J., Crepp, J., and Ge, J., ApJ, article # astro-ph/0411077 (2004).

[8] G. Foo, D.M. Palacios, G.A. Swartzlander Jr., Opt. Lett. **30**, 3308 (2005).

Downloaded From: https://www.spiedigitallibrary.org/conference-proceedings-of-spie on 02 Mar 2022
Terms of Use: https://www.spiedigitallibrary.org/terms-of-use

[9] D.M. Palacios and S. Hunyadi, To appear in Optics Letters (2006).

[10] Jae Hoon Lee, Gregory Foo, Eric G. Johnson, and Grover A. Swartzlander Jr., Phys. Rev. Lett. Article # 053901 (2006).

[11] G.A. Swartzlander Jr., Opt. Lett. **31**, 2042 (2006).

[12] D. W. Wilson, R. E. Muller, P. M. Echternach, and J. P. Backlund, Proceedings of SPIE, **5720**, 68 (2005).

[13] Z. G. Chen, M. Segev, D. W. Wilson, R. E. Muller, and P. D. Maker, Opt. Lett. **22,** 1751 (1997).

[14] Z. G. Chen, M. Segev, D. W. Wilson, R. E. Muller, and P. D. Maker, Phys. Rev. Lett. **78**, 2948 (1997).

[15] L.M. Pismen, *Vortices in Nonlinear Field*s, Oxford Science Publications (Clarendon Press, Oxford, 1999).

[16] Sheldon Green eds., *Fluid Vortices*, (Kluwer Academic Publishers, Dordrecht, Netherlands, 1995).

[17] M. Vasnetsov and K. Staliunas, eds., *Optical Vortices*, vol. 228, Horizons in World Physics, (Nova Science, Huntington, NY, 1999).

[18] G.A. Swartzlander Jr., Opt. Lett. **26**, 497 (2001).

[19] F.B. Colstoun, G. Khitrova, A.V. Fedorov, T.R. Nelson, C. Lowery, T.M. Brennan, B.G. Hammons, and P.D. Maker, Chaos, Solitons, & Fractals **4**, 1575 (1995).

[20] J.D. Jackson, *Classical Electrodynamics*, (John Wiley and Sons, NY, 1962).

[21] Green, J.J., and Shaklan, S.B., Proc. SPIE **5170**, 25 (2003).

[22] D. Mawet, P. Riaud, O. Absil, and J. Surdej, ApJ. **633**, 1191 (2005).

Downloaded From: https://www.spiedigitallibrary.org/conference-proceedings-of-spie on 02 Mar 2022
Terms of Use: https://www.spiedigitallibrary.org/terms-of-use

FIGURES

FIG. 1 A three dimensional plot of an optical vortex mask of topological charge m. The thickness of the mask (the z dimension) increases in the azimuthal direction forming a spiral shape on the upper surface of the mask. The thickness of the mask is represented by the phase shift through the mask in radians.

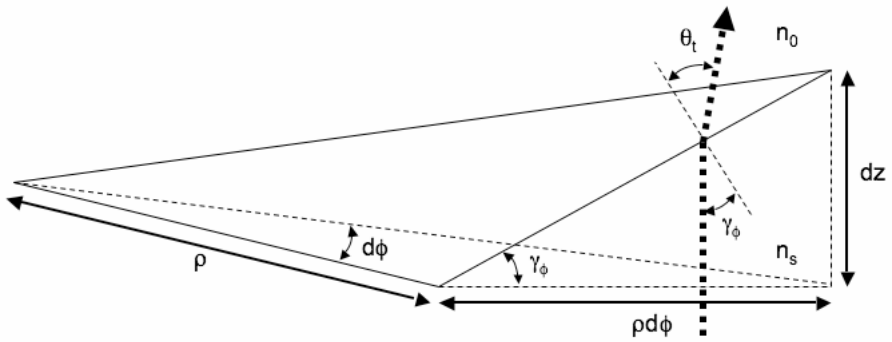

FIG. 2 A ray diagram of light transmission through an azimuthal wedge of an optical vortex mask. The thickness (dz) of the wedge increases as the angular width of the wedge (dϕ) increases in the azimuthal direction. A ray (dashed arrow) is perpendicularly incident on the mask at a radial position ρ. The ray is transmitted through the mask substrate of refractive index n_s and is incident on the spiral front surface of the mask at an angle γ_ϕ from the surface normal. The ray refracts at an angle θ_t from the surface normal into the surrounding medium of refractive index n_0.

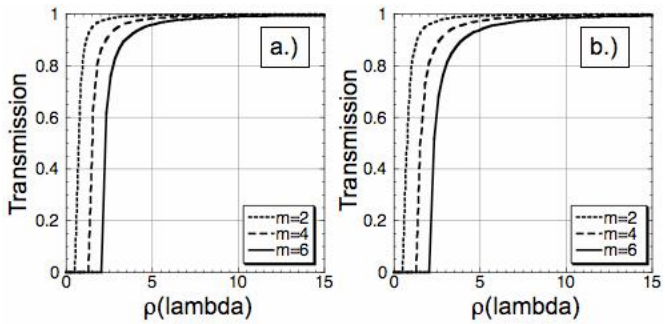

FIG. 3 Radial line plots of the amplitude transmission of optical vortex masks of topological charge, m=2,4,and 6 for a.) radially polarized light and b.) azimuthally polarized light.

Downloaded From: https://www.spiedigitallibrary.org/conference-proceedings-of-spie on 02 Mar 2022
Terms of Use: https://www.spiedigitallibrary.org/terms-of-use

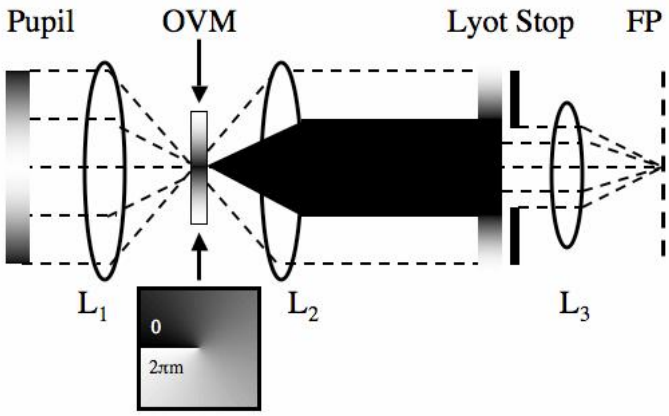

FIG. 4 A simple unfolded model of an optical vortex coronagraph. Lens (L_1) represents the telescope optics, which focus the light from the entrance pupil onto an optical vortex mask (OVM) of topological charge, m. Lens (L_2) collimates the light forming an exit pupil where a Lyot stop is placed. A third lens (L_3) re-images the light to the final image at (FP).

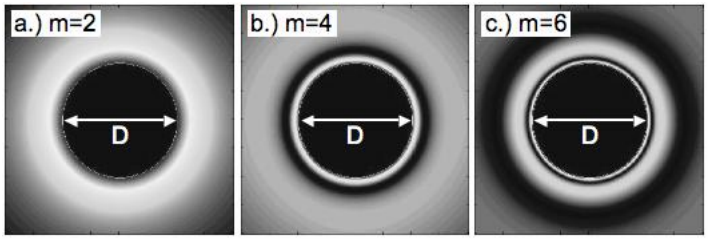

FIG. 5 Images of the Lyot plane of an optical vortex coronagraph with an optical vortex mask of topological charge a.) m=2, b.) m=4, and c.) m=6. The residual stellar light is redistributed outside the pupil of diameter, D.

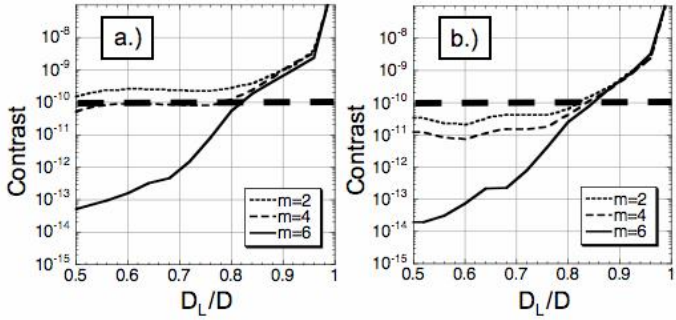

FIG. 6 Plots of the contrast averaged between a.) 2-3λ/D and b.) 4-5λ/D vs. Lyot stop diameter, D_L, for optical vortex coronagraphs of topological charge, m=2,4 and 6. The Lyot stop diameter is normalized by the pupil diameter, D. The thick dashed line at 10^{-10} represents the contrast requirement of the Terrestrial Planet Finder Mission.

Downloaded From: https://www.spiedigitallibrary.org/conference-proceedings-of-spie on 02 Mar 2022
Terms of Use: https://www.spiedigitallibrary.org/terms-of-use

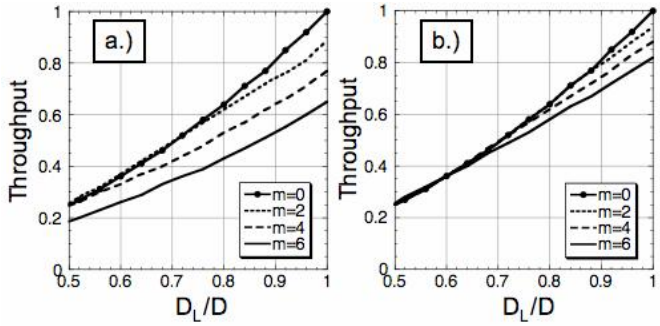

FIG. 7 Plots of the planet light throughput for a planet located at a.) 2λ/D and b.) 4λ/D vs. Lyot stop diameter, D_L, for optical vortex coronagraphs of topological charge, m=0,2,4 and 6. The Lyot stop diameter is normalized by the pupil diameter, D. The m=0 case represents the throughput limited by the Lyot stop without an optical vortex mask present.

Downloaded From: https://www.spiedigitallibrary.org/conference-proceedings-of-spie on 02 Mar 2022
Terms of Use: https://www.spiedigitallibrary.org/terms-of-use